Hydrodynamic interactions between rotating helices

MunJu Kim and Thomas R. Powers*
Division of Engineering, Box D, Brown University, Providence, Rhode Island 02912, USA
(Received 5 July 2003; revised manuscript received 20 January 2004; published 4 June 2004)

Escherichia coli bacteria use rotating helical flagella to swim. At this scale, viscous effects dominate inertia, and there are significant hydrodynamic interactions between nearby helices. These interactions cause the flagella to bundle during the "runs" of bacterial chemotaxis. Here we use slender-body theory to solve for the flow fields generated by rigid helices rotated by stationary motors. We determine how the hydrodynamic forces and torques depend on phase and phase difference, show that rigid helices driven at constant torque do not synchronize, and solve for the flows. We also use symmetry arguments based on kinematic reversibility to show that for two rigid helices rotating with zero phase difference, there is no time-averaged attractive or repulsive force between the helices.

DOI: 10.1103/PhysRevE.69.061910 PACS number(s): 87.16.Qp, 47.15.Gf, 87.19.St

I. INTRODUCTION

In hydrodynamics at the micron scale, viscous damping determines the characteristics of the flow, and inertia is irrelevant [1]. Consequently, microorganisms cannot swim by imparting momentum to the fluid. Instead, their propulsion mechanisms are based on designs which are fundamentally different from schemes exploited by macroscopic organisms. For example, bacteria such as *Escherichia coli* swim by rotating thin helical propellers [2] which would be hopelessly inefficient at the macroscopic scale. The thrust generated by a bacterial flagellum arises from viscous drag. A second striking feature of fluid mechanics in the viscously dominated regime, or equivalently, at low Reynolds number, is the long range of hydrodynamic interactions. For example, the Stokeslet, or flow field induced by a point force, falls off inversely with distance [3]. This effect has been argued to be important for the patterns of feeding currents in choanoflagellates [4], the metachronal waves of ciliary beat patterns in *Paramecium* [5], and the bundling of bacterial flagella [6].

In this paper we study the role of hydrodynamic interactions in a toy model for the flagella of bacteria such as *E. coli* and *Salmonella* (see Ref. [2] for a review). These cells have four to ten flagella per cell. Each flagellum consists of a rotary motor; a universal joint about 50 nm long, known as the hook, and a helical filament 20 nm in diameter and about 10 μm long. The motor rotates the filament at roughly 100 Hz. In the wild type, the filaments have the left-handed "normal" form in the absence of external stress, with a pitch of about 2.28 μm and a helical diameter of 0.37 μm [7]. The helices are flexible enough that viscous stresses can cause them to wrap around each other and also cause polymorphic transformations during chemotaxis [7]. Here for simplicity we disregard flexibility, and focus on hydrodynamic interactions by considering two rotating *rigid* helices. We suppose the helices are driven by stationary motors, as when the cell body is stuck to a wall such as a microscope slide. However, for simplicity, we ignore the effect on the flow of the no-slip boundary condition at the wall; in our calculation, its only role is to provide external forces and torques on the helices. Although the neglect of flexibility and the no-slip condition at the wall are drastic simplifications, our calculations shed light on the hydrodynamic interactions between rotating helices in the simplest possible situation. Furthermore, our calculations are the first step towards developing a framework to treat more complicated situations, such as the "bacterial carpet" of Ref. [8] in which the flagella from a dense layer of *Serratia maracens* bacteria adsorbed to a substrate induce complex flows that can lead to enhanced mixing.

In this paper, we begin with a brief review of related work. After describing the model and its parameters, we present symmetry arguments for the time-averaged forces on the helices. In the next section, we describe the numerical results in terms of resistance matrices, and argue that, despite the hydrodynamic interaction, nearby helices driven at constant torque do not entrain each other. Finally, the flows are presented for in-phase and out-of-phase rotation.

For a swimming bacterium, the Reynolds number, $\mathrm{Re}=\rho v L/\eta$, is about 10^{-5}, where $\rho=10^3$ kg/m^3 is the density of water, $v\approx 10$ μm/s is the swimming speed, $L\approx 1$ μm is the size of the cell body, and $\eta=10^{-3}$ N s/m^2 is the viscosity of water. We can therefore model the flow as zero Reynolds number flow, or Stokes flow. The Stokes flow generated by a single rotating and translating helix was calculated by Lighthill in the slender-body approximation [9]. There is no net force on a swimming body. Thus, Lighthill considered an infinite rotating and translating helix subject to zero net force. In more recent work, Ramia *et al.* computed the flows induced by two nearby model swimming microorganisms, which each consisted of a sphere propelled by a rotating helix [10]. For a swimming microorganism, the flow in the far field falls off inversely with the square of distance, since the requirement of zero net force eliminates the Stokeslet from the multipole expansion. However, if an external force prevents the microorganisms from swimming, then the far-field flow decays inversely with distance. Here, we consider two rotating helices which are prevented from translating by an external force. We give a precise, quantitative assessment of the role of hydrodynamic interactions in this key geom-

*Email: mjkim@brown.edu,Thomas_Powers@brown.edu

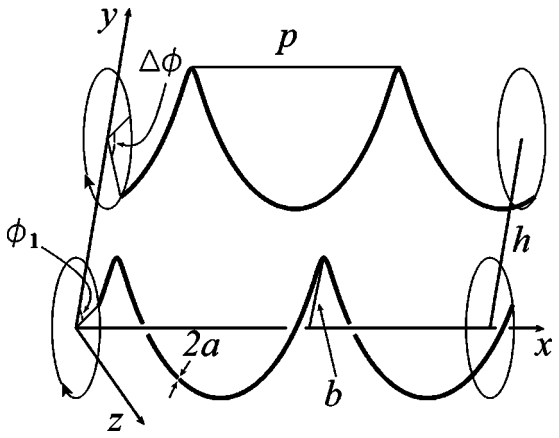

FIG. 1. Two identical rotating helices.

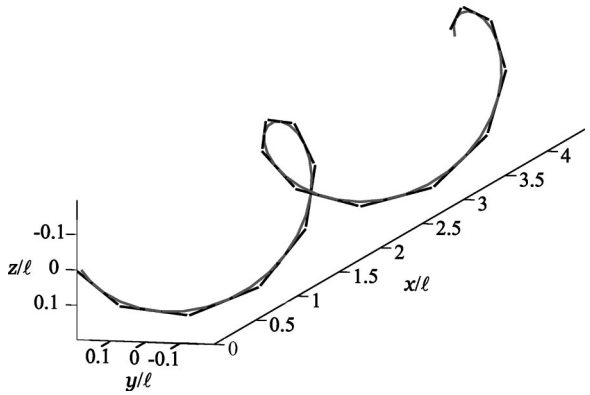

FIG. 2. Line segment approximation of a helix. Only two turns are shown.

etry. Our results are complementary to those of Ramia *et al.*, since the hydrodynamic interactions between our helices are stronger. Our work is also related to that of Higdon, who studied the feeding currents generated by single rotating helix attached to a wall [4].

II. MODEL

Figure 1 defines the parameters of our model. Two identical helices with amplitude b, pitch p, and rod radius a rotate with speeds ω_1 and ω_2. The x axis coincides with the axis of the first helix; both axes lie in the xy plane. The helices have four turns; only two are shown. Since the helices are rigid, their axes are parallel with constant separation h. In this paper we study helices with the dimensions of the normal wave form, given in the Introduction. We focus on nearby helices, with $h=3b$. The centerlines of the helices are parametrized by

$$\mathbf{X}_1(s,t) = (\alpha s, b\,\cos(ks+\phi_1), b\,\sin(ks+\phi_1))$$

$$\mathbf{X}_2(s,t) = (\alpha s, b\,\cos(ks+\phi_2)+h, b\,\sin(ks+\phi_2)), \quad (1)$$

where $\alpha = p|k|/(2\pi)$, $k=-[b^2+p^2/(4\pi^2)]^{-1/2}$, $\phi_1=\omega_1 t$, $\phi_2=\omega_2 t+\Delta\phi_0$, $\Delta\phi_0$ is the initial phase difference, s is arclength, and t is time. Note that $k<0$, since the normal flagella are left-handed. It is convenient to introduce the length unit $\ell = p/2.28$, so that $\ell = 1$ μm.

At $\mathrm{Re}=0$, the flow is governed by the Stokes equations for incompressible flow, $\eta\nabla^2\mathbf{v}=\nabla p$, where $\mathbf{v}$ is the velocity ($\nabla\cdot\mathbf{v}=0$), p is the pressure, and η is the dynamic viscosity. The boundary conditions are $\mathbf{v}\to\mathbf{0}$ far from the helices, and no slip at the surfaces of the helices. Although the Stokes equations are linear, the complex geometry of the rotating helices makes it difficult to solve the equations analytically. We therefore turn to the slender-body approximation [3,11], in which line distributions of point forces (Stokeslets) and source dipoles (doublets) replace the helices. The density of the doublets relative to the Stokeslets is chosen to enforce the no-slip boundary condition around the circumference of the filament at each point s, and the velocity at any point $\mathbf{x}$ is found to $O(ka)$ [3] by linear superposition:

$$v_i(\mathbf{x}) = \sum_{\mu j}\int\left[S_{ij}\frac{f_{\mu j}}{8\pi\eta} - D_{ij}\frac{a^2 f_{\mu\perp j}}{16\pi\eta}\right]ds_\mu, \quad (2)$$

where i and j run over x, y, and z, and μ runs over 1 and 2. In Eq. (2), the integration runs over the arc length of both helices; $\mathbf{f}_\mu=\mathbf{f}_\mu(\mathbf{X}(s))$ is the force per unit length exerted *on* the fluid by the μth helix, $\mathbf{f}_{\mu\perp}$ is the transverse part of $\mathbf{f}_\mu$ ($\mathbf{f}_{\mu\perp}\cdot\partial\mathbf{X}_\mu/\partial s=0$),

$$S_{ij}(\mathbf{x},\mathbf{X}) = \frac{\delta_{ij}}{|\mathbf{x}-\mathbf{X}|} + \frac{(x_i-X_i)(x_j-X_j)}{|\mathbf{x}-\mathbf{X}|^3} \quad (3)$$

is the Stokeslet tensor, and

$$D_{ij}(\mathbf{x},\mathbf{X}) = -\frac{\delta_{ij}}{|\mathbf{x}-\mathbf{X}|^3} + 3\frac{(x_i-X_i)(x_j-X_j)}{|\mathbf{x}-\mathbf{X}|^5} \quad (4)$$

is the doublet tensor. In principle there should be another term in Eq. (2) consisting of a superposition of rotlets, corresponding to the viscous resistance to rotation of each filament element about its local axis [12]. These terms would be the only terms present for a rigid straight rod rotating about its long axis, but not translating. However, for the helices we consider here, the contributions of the rotlets to the torque (and flow) are suppressed relative to the terms kept in Eq. (2) by factors of a^2/b^2, and henceforth disregarded.

To determine the force density $\mathbf{f}(\mathbf{X})$, we consider Eq. (2) for positions $\mathbf{x}$ which lie on the helix surface, such as $\mathbf{x}=\mathbf{X}_\mu+a\mathbf{n}_\mu$, where $\mathbf{n}_\mu$ is the unit normal to the μth helix. Note that the nonzero radius of the filament $a>0$ cuts off the divergences of the singular tensors of Eqs. (3) and (4). Thus Eq. (2) becomes an integral equation, since the no-slip condition determines $\mathbf{v}$ at the helix surface. To solve Eq. (2), we approximate each helix as a series of straight rods with length q and radius $a=\ell/100$, corresponding to $a=10$ nm (see Fig. 2) [11]. Then the integral equation (2) becomes a matrix equation, which we solve numerically. The axis of each rod is tangent to the centerline of the helix at the middle of the rod. There is a range of optimal choices for the number N of straight rods, and thus q. If the number of straight rods is too small, the geometry of the helix will be poorly approximated. If the number of straight rods is too large, then the rods will not be long and thin (since a is fixed). For

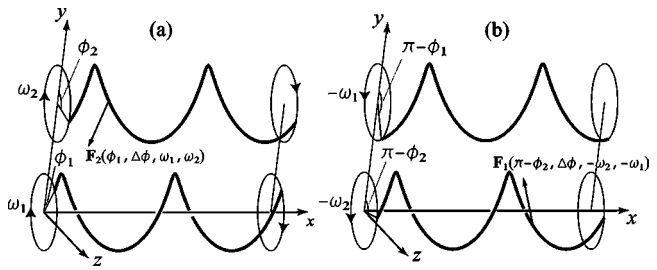

FIG. 3. (a) Reference configuration. (b) The two helices after rotation about the z axis by π and translation along y by h, but *before* reversing the rotation speeds.

the normal, four-turn helix we chose $N=33$, which leads to $a/q \sim 1/30$. As shown in Fig. 2, this choice closely approximates the helix. To validate this approach and our choice of a/q, we considered a ring falling through a highly viscous fluid, where the velocity is perpendicular to the plane of the ring. This case is simple enough to solve analytically; we found excellent agreement between our numerical calculations and the analytic solution. Once $\mathbf{f}(\mathbf{X})$ is determined, we can use Eq. (2) to evaluate the fluid velocity at any point $\mathbf{x}$.

III. SYMMETRY ARGUMENTS

Before we present the numerical results, we use symmetry to relate the time-averaged forces and moments exerted on the fluid by two identical rotating helices. The argument relies upon the principle of kinematic reversibility of Stokes flow, which holds that reversing the direction of motion of the boundaries causes the reversal the velocity of every fluid element as well as the hydrodynamic forces and torques acting on any surface [13].

Also, since in Stokes flow the velocity field depends on the instantaneous position of the boundaries only, the force $\mathbf{F}_\mu$ exerted by each helix on the fluid depends on time only through the phase ϕ_1 of the helix $\mathbf{X}_1$ and the phase difference $\Delta\phi \equiv \phi_2 - \phi_1$: $\mathbf{F}_\mu = \mathbf{F}_\mu(\phi_1, \Delta\phi, \omega_1, \omega_2)$ (for fixed h), where $\mu = 1$ or 2. Note that the $\mathbf{F}_\mu$ are periodic in ϕ_1 and $\Delta\phi$ with period 2π. We assume that the helices have a whole number of turns. If we rotate the helices by π about the z axis, then translate along the y axis by h (see Fig. 3), and finally reverse the directions of rotation of both helices, then by kinematic reversibility and the rules for transformation of vectors under rotations and translations we have

$$F_{1x}(\pi - \phi_2, \Delta\phi, \omega_2, \omega_1) = F_{2x}(\phi_1, \Delta\phi, \omega_1, \omega_2),$$

$$F_{1y}(\pi - \phi_2, \Delta\phi, \omega_2, \omega_1) = F_{2y}(\phi_1, \Delta\phi, \omega_1, \omega_2),$$

$$F_{1z}(\pi - \phi_2, \Delta\phi, \omega_2, \omega_1) = -F_{2z}(\phi_1, \Delta\phi, \omega_1, \omega_2). \quad (5)$$

The net effect of these transformations is the same as rotating each helix about its axis by $\pi - \phi_1 - \phi_2$. Furthermore, if both helices rotate at the same speed ω, then $\Delta\phi$ is constant and the time average of a force over a period is the average of the force over one of the phases, $\langle \mathbf{F}_1 \rangle \equiv \omega/(2\pi) \int \mathbf{F}_1 dt = \int \mathbf{F}_1 d\phi_1/(2\pi)$. Thus

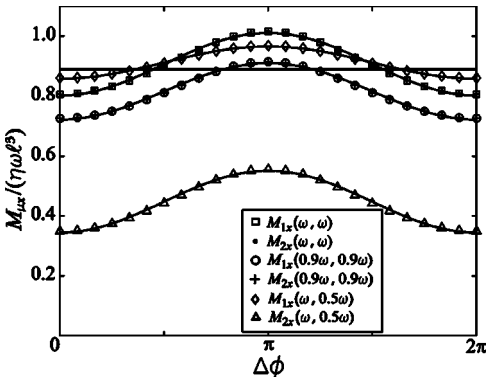

FIG. 4. Torque versus phase difference for $h=3b$. The symbols in the legend correspond to direct numerical calculation. The solid flat line is the torque on a single isolated helix turning at speed ω; the other solid lines correspond to the analytic forms for the $\overline{A_{\mu\nu}}$ described in the text.

$$\langle (F_{1x}, F_{1y}, F_{1z}) \rangle = \langle (F_{2x}, F_{2y}, -F_{2z}) \rangle, \quad (6)$$

where the argument of each component of force in Eq. (6) is $(\phi_1, \Delta\phi_0, \omega, \omega)$.

When the helices rotate at the same speed and have $\Delta\phi = \Delta\phi_0 = 0$, then a similar argument implies that there is no y-component of the time-averaged force exerted by each helix. Rotating the helices about the y axis, translating by their length along the x axis, reversing the direction of rotation of each helix, and averaging over ϕ_1 with $\omega_1 = \omega_2 = \omega$ (with the appropriate changes of variables) yields

$$\langle F_{1y}(\phi_1, -\Delta\phi_0, \omega, \omega) \rangle = -\langle F_{1y}(\phi_1, \Delta\phi_0, \omega, \omega) \rangle, \quad (7)$$

or $\langle F_{1y} \rangle = 0$ for $\Delta\phi_0 = 0$. Similar arguments lead to relations among the moments (relative to the centers) $\mathbf{M}_\mu \equiv \int [\mathbf{X}_\mu(s_\mu, t) - \mathbf{C}_\mu] \times \mathbf{f}_\mu(s_\mu) ds_\mu$ [where $\mathbf{C}_1 = (0,0,0)$ and $\mathbf{C}_2 = (0,h,0)$]:

$$\langle (M_{1x}, M_{1y}, M_{1z}) \rangle = \langle (M_{2x}, -M_{2y}, -M_{2z}) \rangle. \quad (8)$$

Also, these symmetry arguments can be used to show that the tipping torque $\langle M_{1y} \rangle = -(H/2) \langle F_{1z} \rangle$, where H is the axial (not contour) length of each helix. This result can also be derived immediately by observing that in our approximation, all moments on the helices arise from the forces $\mathbf{F}_\mu$.

IV. RESISTANCE MATRICES

We now consider the time dependence of the x components of the torque and force. By the linearity of the Stokes equations,

$$\begin{pmatrix} M_{1x} \\ M_{2x} \end{pmatrix} = \eta \ell^3 \begin{pmatrix} A_{11} & A_{12} \\ A_{21} & A_{22} \end{pmatrix} \begin{pmatrix} \omega_1 \\ \omega_2 \end{pmatrix}, \quad (9)$$

where the $A_{\mu\nu}$ are functions of ϕ_1 and $\Delta\phi$ (for fixed separation h). The reciprocal theorem [13] applied to Eq. (9) with the flows induced by $(\omega_1 = \omega, \omega_2 = 0)$ and $(\omega_1 = 0, \omega_2 = \omega)$ implies that $A_{12}(\phi_1, \Delta\phi) = A_{21}(\phi_1, \Delta\phi)$. Direct computation using the numerical slender-body technique reveals that the $A_{\mu\nu}$ depend weakly on phase ϕ_1; for example, the moments

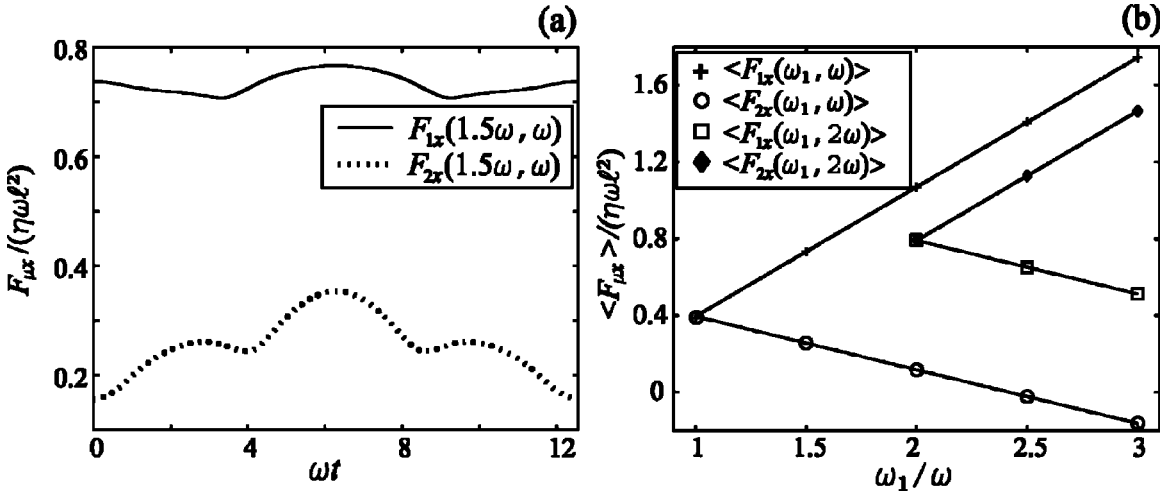

FIG. 5. (a) Time dependence of F_{1x} and F_{2x} for $\omega_1=1.5\omega_2$. (b) Time-averaged axial components of the force.

vary by less than 1% as the phase is varied for fixed phase difference and $\omega_1=\omega_2$. Therefore, since the same symmetry arguments which led to Eq. (5) imply $M_{1x}(\pi-\phi_2,\Delta\phi,\omega_2,\omega_1)=M_{2x}(\phi_1,\Delta\phi,\omega_1,\omega_2)$, we have $M_{1x}(\omega_2,\omega_1)\approx M_{2x}(\omega_1,\omega_2)$, or $A_{11}\approx A_{22}$. For each phase difference, we average the torques over the phase ϕ_1: $\overline{A}_{11}=\int d\phi_1 A_{11}/(2\pi)$. To an excellent approximation (see Fig. 4), our numerical results are captured by the analytic forms $\overline{A}_{11}=\overline{A}_{22}=a_1-b_1\cos(\Delta\phi)$ and $\overline{A}_{12}=\overline{A}_{21}=a_2-b_2\cos(\Delta\phi)$, where a_1, a_2, b_1, and b_2 take the values $a_1=0.9181$, $a_2=-0.0113$, $b_1=0.0029$, and $b_2=0.1017$ for $h=3b$. As h increases, a_2, b_2, and b_1 approach zero, and a_1 approaches the resistance coefficient for a single isolated helix, $a_1=0.8904$.

When the rotation speeds are equal, the phase difference is constant in time and the torque on each helix is approximately constant with a small ($<1\%$) fluctuation. For unequal rotation speeds, $\omega_1\neq\omega_2$, the phase difference $\Delta\phi$ increases linearly with time, and the moments vary sinusoidally about an average value as $\Delta\phi$ changes [see the example $(\omega_1,\omega_2)=(\omega,\omega/2)$ in Fig. 4]. In every case, for constant speeds, the torque is greatest when the helices are out of phase by π, and least when they are in phase.

Our calculations of the moments assume the helices turn at constant speeds; however, the bacterial rotary motor typically runs at roughly constant torque [14]. The cases $\omega_1=\omega_2=\omega$ and $\omega_1=\omega_2=0.9\omega$ of Fig. 4 illustrate the general conclusion that there are many different combinations of speed and phase difference that lead to the same torque. To see how the phase difference evolves, invert the resistance matrix in Eq. (9) and solve for $d\Delta\phi/dt=\omega_2-\omega_1$ to find

$$\eta\ell^3\frac{d\Delta\phi}{dt}=\frac{M_{2x}-M_{1x}}{\overline{A}_{11}-\overline{A}_{12}}. \tag{10}$$

The phase difference is constant only if $M_{2x}=M_{1x}$, in which case $\Delta\phi=\Delta\phi_0$, and the rotation speeds are $\omega_1=\omega_2=M_{1x}/[\eta\ell^3(\overline{A}_{11}+\overline{A}_{12})]$, with $\overline{A}_{11}$ and $\overline{A}_{12}$ evaluated at $\Delta\phi=\Delta\phi_0$. When $M_{2x}\neq M_{1x}$, the phase difference changes continuously, since there is no value of $\Delta\phi$ for which $1/(\overline{A}_{11}+\overline{A}_{12})$ vanishes. Since $|A_{12}|\ll|A_{11}|$, $\Delta\phi$ increases roughly linearly, with small fluctuations due to the hydrodynamic interaction. In contrast to pairs of nearby waving cilia [5] or undulating flagella [15], hydrodynamic interactions do not cause nearby rotating (rigid) helices to synchronize.

The numerical calculations show that, unlike the moments, the axial components of the forces depend on *both* the phase and the phase difference: $F_{\mu x}=\eta\ell^2\Sigma_\mu B_{\mu\nu}(\phi_1,\Delta\phi)\omega_\nu$. Thus the time dependence of the forces is more complicated than the time dependence of the moments [Fig. 5(a)]. However, we can give a simple characterization of the force by averaging over the phase ϕ_1 and the phase difference $\Delta\phi$. This effectively averages over time for many periods. By computing $\langle F_{\mu x}\rangle$ for $\omega_2/\omega_1=1.5$ and $\langle F_{\mu x}\rangle$ for $\omega_2/\omega_1=2$, we found values for $\langle B_{\mu\nu}\rangle$ [solid lines of Fig. 5(b)] which accurately captured the average forces calculated by direct numerical simulation for a range of ω_1 and ω_2 [symbols in legend of Fig. 5(b)]. When $\omega_1=\omega_2$, $\eta\ell^2\Sigma_\mu\langle B_{\mu\nu}\rangle\omega_\nu$ gives the force averaged over all phase differences. We find $\langle B_{11}\rangle=\langle B_{22}\rangle=0.677$, and $\langle B_{12}\rangle=\langle B_{21}\rangle=-0.281$, for $h=3b$. A left-handed helix turning with $\omega>0$ pushes fluid along the x axis [Figs. 6(a) and 6(d)], leading to an anchoring force (the force required to hold the helix, or equivalently, the force the helix exerts on the fluid) in the positive x direction. Thus $\langle B_{11}\rangle=\langle B_{22}\rangle>0$. On the other hand, since a nearby left-handed helix turning with $\omega>0$ also pushes fluid along the x axis, the part of the anchoring force on the helix $\mathbf{X}_1$ due to the flow induced by the helix $\mathbf{X}_2$ is in the *negative* x direction: $\langle B_{12}\rangle=\langle B_{21}\rangle<0$. The magnitude of the axial force on each of two nearby helices rotating with speed ω is less than the magnitude of the axial force on a single helix turning with rate ω in isolation.

V. FLOWS

Once the force F is known, Eq. (2) allows us to calculate the flow field. Figure 6 shows the components of the flow field in the $z=0$ [Fig. 6(a)] and $x=2p$ [Fig. 6(b)] planes for constant phase difference $\Delta\phi=0$, and in the $x=2p$ [Fig. 6(c)]

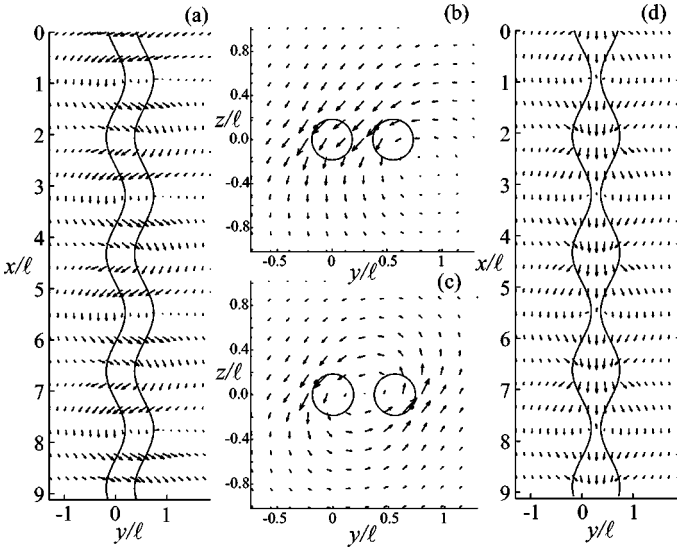

FIG. 6. Flow fields for two left-handed helices rotating with the same angular velocity $\omega=\omega\hat{\mathbf{x}}$.

and $z=0$ [Fig. 6(d)] planes for constant phase difference $\Delta\phi=\pi$. Both helices are left handed and rotate in the same direction; note that the path lines are right handed. The shear rate is highest for $\Delta\phi=\pi$ in the regions where the helices are closest [Fig. 6(c)], which explains why $\Delta\phi=\pi$ has the highest resistive torque for a given speed.

VI. CONCLUSION

Using numerical slender-body calculations and symmetry arguments, we have calculated the hydrodynamic forces and moments on nearby rotating helices at zero Reynolds number. Our results show that rigid helices driven at constant torque do not become entrained. We also presented the flow fields for the two extremes of $\Delta\phi=0$ and $\Delta\phi=\pi$. Although it is difficult (but not impossible) to measure the flow field around rotating flagella, all of our results can be tested in a scale-model experiment such as that described in Ref. [6]. As mentioned in the Introduction, our results do not directly apply to swimming bacteria since our helices are prevented from translating. Instead, our results are relevant for understanding interactions between rotating flagella in a situation like the "carpet" of bacteria studied by the authors of Ref. [8]. The next challenge is to include the flexibility of the flagella (see Ref. [16]), since the forces we describe in this article will cause the flagella to deflect and form a bundle (for the proper rotation sense) [6]. Another extension of the results described in this article would be to consider two rotating rigid helices with noncoplanar axes. The new element in this configuration may be a steady attractive (or repulsive) force between the two helices. We will study this situation in future publication.

ACKNOWLEDGMENTS

We thank H. Berg, K Breuer, N. Darnton, G. Huber, and L. Turner for discussions and collaborations. This work was supported by NSF Grant No. CMS-0093658 and the DARPA BioMolecular Motors Program.

[1] E. M. Purcell, Am. J. Phys. **45**, 3 (1977).
[2] R. M. Macnab, in *Eschericia coli and Salmonella*, edited by F. C. Neidhardt *et al.* (American Society for Microbiology, Washington, D.C., 1996), p. 123.
[3] J. Lighthill, SIAM Rev. **18**, 161 (1975).
[4] J. L.L. Higdon, J. Fluid Mech. **94**, 305 (1979).
[5] S. Gueron and K. Levit-Gurevich, Biophys. J. **74**, 1658 (1998).
[6] M. J. Kim, J. C. Bird, A. J. Van Parys, K. S. Breuer, and T. R. Powers, Proc. Natl. Acad. Sci. U.S.A. **100**, 15 481 (2003).
[7] L. Turner, W. S. Ryu, and H. C. Berg, J. Bacteriol. **182**, 2793 (2000).
[8] N. Darnton, L. Turner, K. S. Breuer, and H. C. Berg, Biophys. J. **86**, 1863 (2004).
[9] J. Lighthill, J. Eng. Math. **30**, 35 (1996).
[10] M. Ramia, D. L. Tullock, and N. Phan-Thien, Biophys. J. **65**, 755 (1993).
[11] J. L.L. Higdon, J. Fluid Mech. **90**, 685 (1979).
[12] W. B. Russel, D. A. Saville, and W. R. Schowalter, *Colloidal Dispersion* (Cambridge University Press, Cambridge, England, 1989).
[13] C. Pozrikidis, *Boundary Integral and Singularity Methods for Linearized Viscous Flow* (Cambridge University Press, Cambridge, England, 1992).
[14] X. Chen and H. C. Berg, Biophys. J. **78**, 1036 (2000).
[15] K. E. Machin, Proc. R. Soc. London, Ser. B **158**, 88 (1963).
[16] H. Flores, E. Lobaton, S. Méndez-Diez, S. Tlupova, and R. Cortez (unpublished).